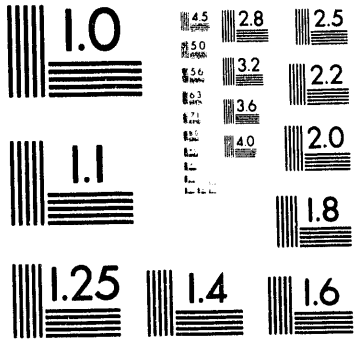
1.0
1.1
1.25
1.4
1.6
1.8
2.0
2.2
2.5
2.8
3.2
3.6
4.0
4.5
5.0
5.6
6.3
7.1

1 of 1

SAND--92-2812C
Conf-930616--30

OBSERVATION OF REFLECTED WAVES ON THE SABRE POSITIVE POLARITY INDUCTIVE ADDER MITL*

M. E. Cuneo, J. W. Poukey, C. W. Mendel, S. E. Rosenthal, D. L. Hanson, J. R. Smith,†
J. E. Maenchen, D. F. Wenger and M. A. Bernard††
Sandia National Laboratories
P. O. Box 5800, Albuquerque, NM 87185-5800

Abstract

We are studying the coupling of extraction applied-B ion diodes to Magnetically Insulated Transmission Lines (MITLs) on the SABRE (Sandia Accelerator and Beam Research Experiment, 6 MV, 300 kA) positive polarity inductive voltage adder. Our goal is to determine conditions under which efficient coupling occurs. The best total power efficiency for an ideal ion diode load (i.e., without parasitic losses) is obtained by maximizing the product of cathode current and gap voltage. MITLs require that the load impedance be undermatched to the self-limited line operating impedance for efficient transfer of power to ion diodes, independent of transit time isolation, and even in the case of a multiple cathode system with significant vacuum electron flow. We observe that this undermatched condition results in a reflected wave which decreases the line voltage and gap electron sheath current, and increases the anode and cathode current in a time-dependent way. The MITL diode coupling is determined by the flow impedance at the adder exit. We also show that the flow impedance increases along the extension MITL on SABRE. Experimental measurements of current and peak voltage are compared to analytical models and TWOQUICK 2.5-D PIC code simulations.

Introduction

The technologies of the inductive cavity and magnetically insulated transmission line (MITL) have been combined as the basis of several high-voltage, high-current particle accelerators (HELIA, HERMES III, and SABRE) at SNL [1]. Voltage addition is achieved in series by stacking inductively isolated cavities along a MITL. Self-magnetic insulation inhibits electron flow across the vacuum gap of the transmission line which would result in shorting (electrons are emitted at high cathode electric fields > 200 kV/cm). A coaxial center conductor threads the bore of the cavities and is stepped to a smaller radius at each cavity gap to match the total drive impedance as the voltage increases along the MITL. In negative polarity (the center conductor is the cathode) this technology has been used to drive intense bremsstrahlung sources for weapons effects testing [2]. In positive polarity (the center conductor is the anode), this technology has also been used to drive ion diodes for ion fusion research [3]. SABRE is a ten-cavity linear induction adder [4] constructed to investigate issues relevant to inertial confinement fusion, target standoff, and ion beam focusing for a Laboratory Microfusion Facility (LMF). These issues include accelerator and MITL physics, MITL to diode coupling, ion sources, and beam divergence and transport. SABRE is currently configured to provide 6 MV and 300 kA to a 4.2 m long coaxial output transmission line terminated in an applied-B extraction ion diode [5].

In this paper we report on experimental and theoretical studies of the MITL-to-diode power coupling, an important element of LMF system performance. The physics of single and multiple-cathode MITLs and simple models describing their behavior will be discussed in the remainder of the introduction. The experimental configuration and diagnostics will be described. The data will then be discussed in context of those models and compared briefly to simulation results.

Single Cathode MITL Physics and Reflected Waves

In the negative polarity operation of an inductive adder, the center cathode is one continuous conductor. The operating impedance of a magnetically insulated transmission line (MITL) with a single cathode is well understood [6,7]. After electrons have been emitted, the operating impedance is reduced below the vacuum impedance of the line due to the presence of space charge.

Mendel [6,7] derives an expression relating the line voltage V_{line} to the anode and cathode currents, I_a and I_c given by

$$V_{line} = Z_o(I_a^2 - I_c^2)^{1/2} - (mc^2/2e)(I_a^2/I_c^2 - 1) \quad (1)$$

where Z_o is the vacuum impedance of the transmission line. Eq. 1 will be referred to as the single cathode (SK) model. At SABRE voltages, Eq. 1 gives results which are essentially equivalent to Creedon's parapotential formulation [8]. A useful expression to evaluate properties of the general, time-dependent flow is given by

$$V_{line} = Z_f(I_a^2 - I_c^2)^{1/2} \quad (2)$$

where Z_f is defined as the "flow impedance" [9,10] a measure of the extent of the electron sheath into the anode-cathode gap.

At a fixed voltage, Eq. 1 predicts the existence of a minimum anode current I_{amin}. The self-limited operating impedance of the MITL, Z_{sl}, is often defined as V_{line}/I_{amin} at the particular voltage of interest. The incident wave operates at the self-limited impedance for times before the power has reached the diode. This regime is referred to as line-dominated behavior. The flow impedance Z_f in Eq. 2 is analogous to Z_{sl}. Previous work [2,11,12] has shown the transition from line-dominated to load-dominated regimes as the net load impedance (MITL + diode) decreases below Z_{sl}. When the net load impedance falls below Z_{sl}, a reflected wave is launched from the load [12-15] and returns upstream, communicating the load conditions back up the MITL. The increase in cathode current accompanying the reflected wave is mostly displacement current but also includes some electron (particle) current returning to the cathode and is the subject of ongoing work [16].

The reflected wave causes a non-zero electric field at the cathode, different from the assumptions of Eq. 1 and Eq. 2. These equations therefore require modification in the presence of a reflected wave, although the corrections may be small. These equations (or if necessary, a generalization taking into account non-zero cathode electric field) can describe the equilibrium state that exists on either side of the transient reflected wave: line dominated (self-limited) ahead of the wave and load-dominated behind the wave. They predict that the anode and cathode currents both increase, and the difference between them, the electron sheath current, decreases. Larger cathode currents are desirable for an ion diode load, which can convert only the current delivered in the cathode into ions.

Multiple Cathode MITL Physics

In a positive polarity induction adder, *each* of the induction cavities is a cathode emitting electrons of unique energy and axial canonical momentum into the vacuum electron flow [17]. As shown by Rosenthal [17], this results in a thick electron layer that strongly affects the MITL behavior making the flow markedly different from that in single cathode MITLs. The case of "full-gap-flow" (FGF) [17] with $Z_f = Z_o/2$ in Eq. 2 matched the results at the adder output of HERMES III positive polarity experiments [18] well. Eq. 2 is an exact analytic relation between V, I_a and I_c for the case of a uniform density electron sheath entirely filling a planar MITL anode-cathode gap. Ref. [17] also suggested that a particular application of Eq. 1 called the "locally-emitted-flow" (LEF) model yielded a good estimate of line voltage. This model assumes that the electrons emitted from the lower voltage cathodes follows equipotentials sufficiently distant from the final cathode that their space charge does not significantly reduce its emission. Recent work on a "layered-flow" model has generalized this approach [19].

*Work supported by the U.S. Dept. of Energy, Contract No. AC04-76DP00789.
†Titan/Spectron, ††Ktech Corporation

DISCLAIMER

The following features of multiple cathode operation have been observed in simulations and experiments on positive polarity inductive adders:

Table I - Observed Characteristics of Positive Polarity Adders

(A) The electrons not emitted at full energy represent a net current (and energy) loss [18] unless the diode is strongly undermatched, and this additional vacuum electron flow reduces the current transport efficiency (I_c/I_a) to the end of the adder in comparison to negative polarity operation [11,17,18] of an inductive adder.

(B) The thick electron layer lowers the operating impedance of the MITL because of the additional amount and spatial extent of space charge [11,17], decreasing the cavity-to-MITL power coupling efficiency [11,17,18] and reducing the MITL-to-diode power coupling efficiency compared to negative polarity.

It is imperative to understand the details of the electron flow, particularly how it modifies the MITL operating impedance which ultimately determines maximum possible load power.

Experimental Configuration

The SABRE inductive voltage adder consists of two sets of five cavities. Each cavity in the accelerator is charged to a nominal 750 kV. Each set of five cavities is charged through an electrically triggered gas switch. Firing of the switch on the downstream set is delayed (nominally by 11 ns) to compensate for the wave transit time between the two cavity sets. The two sets of cavities and connecting transmission line make up the 5.5 meter long adder section. Further details of the SABRE pulsed power and adder section configuration are given in Ref. [4]. The adder drives a 4.2 meter long coaxial extension MITL section with Z_o = 40 Ω (one way transit time to diode = 14 ns at the speed of light, c). That transit time isolates the diode from most of the machine for the majority of the pulse. The coaxial extension MITL is terminated with an applied-B extraction ion diode [5] and a diagnostic spool (see Fig. 1) containing two time-resolved voltage diagnostics, a peak voltage monitor, and anode and cathode current diagnostics, as described below.

B-dot loops and current shunts are used to measure the anode and cathode current at about 10 axial locations along the 9.7 m long adder and extension. Each monitor consists of a pair of signal pickups configured for common mode noise rejection. At each axial location, a set of two anode (inner electrode) and two cathode (outer electrode) B-dots, 180° apart are measured and averaged. The B-dots are calibrated in place by comparison with the pre-calibrated current shunts on short

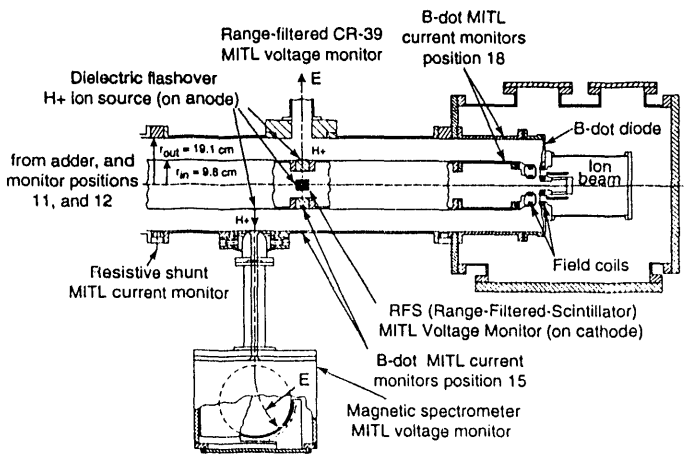

Figure 1. Extraction ion diode load and diagnostic spool configuration, which terminates the 4.2 m long, coaxial extension MITL, with radii as shown. The voltage and current diagnostics shown are at or near position 15; position 18 is just before the diode gap. The adder and extension monitor positions 11, and 12 are upstream, to the left of the figure. The voltage diagnostics measure the energy, E, of protons accelerated across the MITL gap by several different techniques.

circuit shots. The difference between the anode and cathode B-dots is the instantaneous electron sheath current flowing in the MITL gap. When coupled with voltage measurements, these currents allow direct comparisons with Eq. 1 and 2 or similar models. The voltage is obtained by measuring the energy of protons accelerated across the MITL gap using several different techniques. In this paper we will discuss only current measurements just before the last cavity and in the extension MITL, and peak voltage data from the two range-filtered diagnostics shown in Fig. 1 [20].

Experimental Data, Simulation Results and Discussion

Anode (inner MITL) B-dot signals are obscured by current injection into the cables from electron loss through the inner MITL wall before self-magnetic insulation is established. The cathode B-dots have good signal to noise and show no improvement with common mode rejection. Low diode impedance limits the period of electron loss to the anode B-dot cables so that "reasonable" anode current data were obtained. "Reasonable" data is where the initial portion of the anode and cathode B-dots agree. Fig. 2 shows anode and cathode current data, and the electron sheath current from: position 11, just before the last cavity; position 12, just after the last cavity in the extension MITL; position 15, downstream of position 12; at position 18 just before the diode B-field return flux; and at the diode gap (cathode current only). The axial distances in m and one way transit times from the diode in ns (at c), for each position are noted on the figure. The prominent features of Fig. 2 are discussed in Table II.

Table II - Experimental Observations

(A) There is a vacuum wave precursor (denoted as p.c.) moving at velocity u = c, during which the anode and cathode currents are equal. The line in Fig. 2 at the beginning of signals of position 12 and 15 shows that velocity. This precursor results from wave propagation prior to MITL electron emission.

(B) The incident wave (denoted as i.w.) velocity is $u_i = 0.8 \pm 0.2$ c based on the timing of the 80 kA level between 12 and 15. The uncertainty is due to a ± 3 ns timing accuracy for this data. Note the line reflecting this velocity in Fig. 2.

(C) There is a large jump in sheath current at the adder end, between positions 11 and 12, corresponding to locally-emitted-flow from the final, full voltage cathode, suggesting that the lower energy electrons do not significantly reduce the equilibrium emission of the final cathode.

(D) There is a period of time after the incident wave arrives at the diode, but before the diode conducts appreciable current when the system is still dominated by the line impedance. After the diode becomes undermatched, a reflected wave (denoted as r.w.) travels upstream, and is successively visible on the monitors at 15, 12, and 11. The velocity of the reflected wave is $u_r = -0.8 \pm 0.2$ c, based on the timing of the 80 kA level between 15 and 12. Note the line indicating this velocity in Fig. 2. The reflected wave is accompanied by a systematic reduction in sheath current with length.

(E) The anode current is also observed to increase at positions 11 and 12 at the time of the reflected wave. At position 15, no apparent increase in the anode current is observed. This may result from current losses between 12 and 15, which are confirmed by noise signals on shorted, integrated cables (with no B-dots) in the inner MITL.

(F) The peak total current at the beginning of the adder is 300 kA. The transport efficiency of peak total current to position 18 is I_{a18}/I_{a1} = 284 kA/300 kA = 95%. The peak cathode current at 18 and at the diode are both 238 kA, showing that all sheath current is lost at the return flux of the applied-B before entering the diode. This observation verifies the assumptions of the model in the last section and is consistent with simulations. The sheath current at peak power at position 18 is 46 kA. The current efficiency of the MITL at position 18 is I_{cdiode}/I_{a18} = 238/284 = 84%, giving a total efficiency of I_{cdiode}/I_{a1} = 238/300 = 79%.

(G) The differences in pulse shape at position 18 between the anode and cathode B-dots in the early portion of the pulse result from electron charge collection in the anode signal cables. The small differences at position 15 imply these data are reasonable. The collection is much greater at position 18 as evidenced by the greater distortion of the leading edge of the anode current (as noted in Fig. 2a). These possible errors in anode current would strongly affect only the conclusions about current efficiency in (F) above.

The vacuum wave precursor described in (A) has been observed at low amplitudes in other long MITL experiments and simulations [12,21]. The amplitude of the precursor (3-4 MV) is significant in the

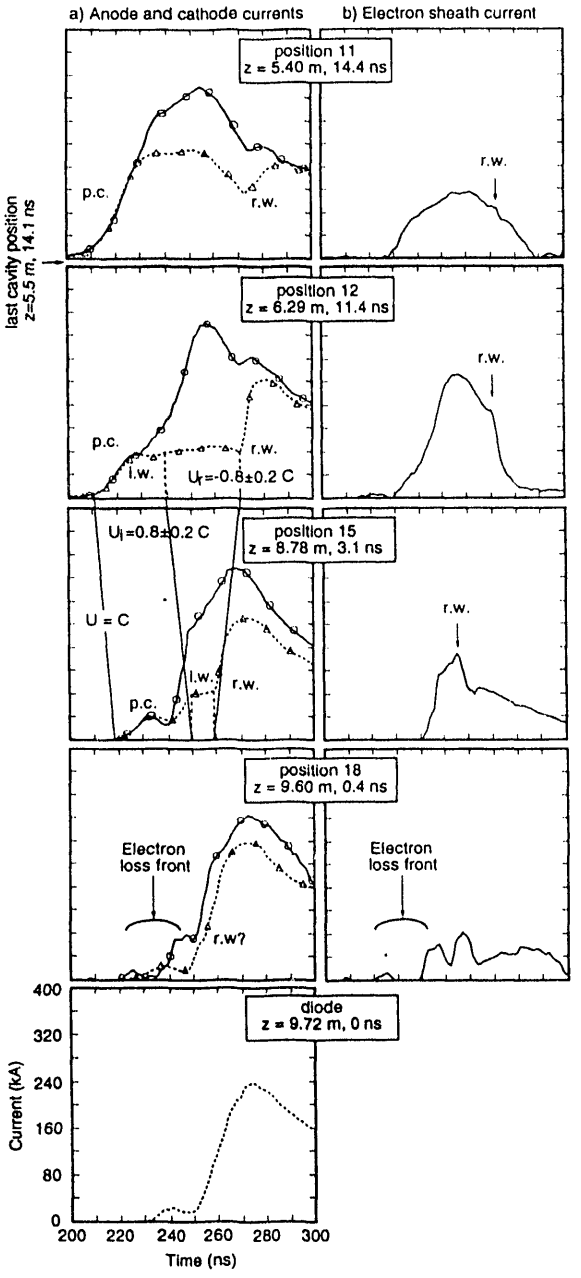

Figure 2a) Left column: Anode (solid lines) and cathode currents (dotted lines) for positions 11, 12, 15, 18 and cathode current at the diode. Note the lines giving schematically the velocities of the precursor (p.c.), incident insulated wave (i.w.), and reflected wave (r.w.). 2b) Right column: The electron sheath current, the difference between the anode and cathode currents in part a) show the systematic reduction in sheath current with length accompanying the reflected wave. The axial location of each of these positions in m, and one way transit time from the diode in ns (at c) is noted on the figure. The last cavity accelerating gap is at z=5.5 m (14.1 ns).

present experiments because the impedance and therefore MITL gaps are relatively large (9.3 cm) hence the threshold for electron emission is not reached until well into the power pulse rise time. Precursor (u=c) and main insulated wave (u<c) separate as they propagate down the long machine. This feature has an important impact on the operation of ion diode loads.

Table III present brief comparisons between observed phenomenon (Table II) and TWOQUICK [22] PIC-code simulations.

Table III - TWOQUICK Simulation Results

(A) The simulations show that a 200 - 300 kV/cm cathode emission threshold and an emission development period of < 5 ns are required to qualitatively match the features of the experimentally observed MITL and diode voltages.

(B) Simulations show u_i = 0.75±0.06 c for the incident wave at V = 4 MV, in agreement with Fig. 2.

(C) The reflected wave velocities are u_r = 0.61±0.09 c at the 110 to 150 kA level, for a range of load impedances near peak power. The amplitude of the reflected wave is larger for lower impedance loads.

(D) The anode current also increases across the reflected wave. These increases are larger for lower load impedances but less dramatic than those in the cathode current.

Voltages determined using the current models of Eq. 1 (V_{SK}), Eq. 2 (V_{ZFL} or V_{FGF}) and the LEF model (V_{LEF}) [17], are compared to experimentally determined peak voltages (V_{FOR}, V_{CR39}) and peak voltages from the simulations (V_{SIM}) in Fig. 3. Upper and lower bounds on the peak forward going voltage at the end of the adder near position 12, (V_{FORU}, V_{FORL}) are estimated using an equivalent accelerator load line determined from the measured pulse forming line voltage and an estimated MITL operating impedance. The experimentally measured peak voltages at position 15 are obtained using the time-integrated range-filtered CR-39 (upper and lower bounds V_{CR39U} and V_{CR39L}).

A comparison of voltages calculated from currents at position 12 (V_{SK}, V_{FGF}, V_{LEF}) to V_{SIM}, V_{FORU}, V_{FORL}, and V_{CR39} is shown in Fig. 3a. The agreement between LEF, FGF, measurement and simulation implies that the flow impedance is close to 20 Ω at the adder exit. A comparison of current based models for position 15 (V_{SK}, V_{ZFL}, V_{FGF}) to V_{CR39U}, V_{CR39L}, and V_{SIM} is shown in Fig. 3b. The agreement is best for a flow impedance model with Z_f = 27 Ω. Since Eq. 2 is an exact definition for Z_f in the incident wave, a measurement of V, I_a and I_c determines Z_f.

Simulations also show an increase of Z_f along the extension MITL with 24.4±1.1 Ω at the adder exit, 29.7±1.3 Ω at position 12, 33.8±2.8 Ω at position 15, and 38.6±3.1 Ω at position 18 (at high diode impedance). These values are higher than the corresponding experimental values, possibly because the simulations show electron loss to the anode in the adder section that is not seen in experiments. Also, the simulations show a faster increase of Z_f with length. These data and simulation results demonstrate that Z_f increases as the wave propagates down the extension MITL, before the reflected wave returns to the monitor position. (It is also found that the Z_f from the simulations is actually fairly constant across the reflected wave.) The increase of Z_f along the extension results from electron loss to the anode reducing charge in the gap, which both simulation and experiment show. Electrons returning to the cathode (before the reflected wave) would also increase the flow impedance, and this is also seen in both experiment (not shown in Fig. 2) and simulation. The differences between simulation and experiment require further investigation.

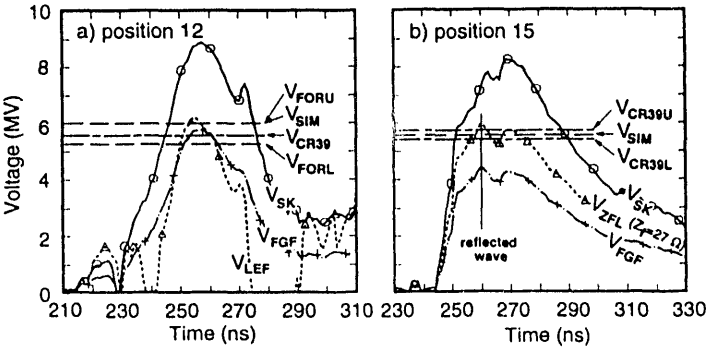

Figure 3a) A comparison of voltages based on current at position 12 (V_{SK}, V_{FGF}, V_{LEF}) to estimated peak forward going voltage at the adder exit (V_{FORU}, V_{FORL}), measured voltage V_{CR39} (measured at position 15), and simulation voltage at position 12 (V_{SIM}). The subscripts U and L refer to upper and lower bounds. Results imply Z_{f12} = 20 Ω. 3b) A comparison of current based models (V_{SK}, V_{ZFL}, V_{FGF}) at position 15 to experimentally measured peak voltage (V_{CR39U}, V_{CR39L}), and simulation voltage at position 15 (V_{SIM}). Agreement implies Z_{f15} = 27 Ω.

Comparisons of Experiment and Simulations to Equilibrium Models

The equilibrium models, Eqs. 1 and 2, are used to investigate new operating points when coupling a MITL to an undermatched diode. The anode (or total) current is determined at a particular line voltage through the accelerator load line, defined by $V_{line} = V_{oceff} - I_a Z_a$, where V_{oceff} is the effective open circuit voltage and Z_a is the accelerator source impedance. The line voltage and anode current determine the cathode current available to an ion diode, through a function of form $V = f(Z, I_a, I_c)$ (given here by Eq. 1 or Eq. 2) with $Z = Z_o$ or Z_f. This approach assumes that sheath current will never couple into an ion beam. The experimental data in Fig. 2 agree with this. This is also verified in simulations of applied-B diodes. This cathode current is the maximum ion current possible if the ion diode were perfectly efficient at converting electrical power into ions. We might expect Eq. 2 to be a better model of multiple cathode MITLs based on Fig. 3 and the work of Rosenthal [10,17,23].

A physically revealing way to view these equilibrium models is to plot the power available (or coupled) at the diode for conversion to ions ($V_{line}I_c$) versus the diode impedance (V_{line}/I_c). The power falls off for large impedances because the cathode current is decreasing faster than the voltage is increasing. At small impedances the voltage is falling faster than can be made up for by increases in the cathode current. Between these two limits there is a broad maximum where the cathode current regained from undermatching offsets the decrease in power from the voltage decrease. These results imply that the open circuit voltage and impedances of an accelerator/MITL/diode system should be chosen to allow the desired voltage be achieved at the impedance giving peak available power.

Fig. 4 shows a comparison of this model for SABRE load line parameters to peak power data from typical SABRE proton and lithium diode shots, and TWOQUICK PIC-code simulations of the SABRE experiments. The largest uncertainty in application of the model is in determining what the effective open circuit voltages is, including inductive effects ($V_{oceff} = V_{oc} - (dI_a/dt)L = V_{line} + I_a Z_a$). Changes in electron loss (for example between simulation and experiment or between different load types) can change the anode current and therefore the effective open circuit voltage. In addition the model is very sensitive to V_{oc}. A + 8% change in V_{oc} (from 15 to 16.2 MV) results in a -28% change in Z_f (from 28 to 20), each case giving the same peak power (1.01 TW). Each of the model curves are therefore shown for a lower bound of V_{oceff} = 15 MV and an upper bound of V_{oceff} = 17 MV. The best agreement between the experimental and simulation data and the model is obtained using the flow impedance at the exit of the adder to describe the coupling to the diode ($Z_f = 20\ \Omega$ for experiment, $Z_f = 24\ \Omega$ for the simulation). The equilibrium model may require modifications for distributed loss, distributed flow and time-dependent effects

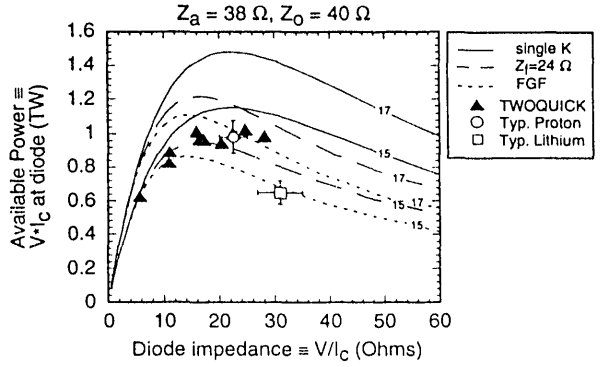

Figure 4. Comparison of equilibrium model for available power at the diode versus diode impedance for Eq. 1 (solid line), and Eq. 2 with $Z_f = 24\ \Omega$ (long dashes), and $Z_f = 20\ \Omega$ (FGF) (short dashes) with SABRE proton (open circle) and lithium (open square) diode data and TWOQUICK simulations (filled triangles). For each model case, the upper bound is V_{oceff} = 17 MV, the lower, V_{oceff} = 15 MV. This model implies a peak power penalty for positive polarity operation of SABRE of greater than 25% compared to negative polarity (single cathode) operation.

when the turn-on and current enhancement of the diode is poor, and the timing of peak ion power, cathode power and forward wave power do not coincide.

The model shows that for lower Z_f, the impedance for maximum power shifts to lower fractions of Z_o ($Z_{pk}/Z_o = 0.375$ at $Z_f = 20\ \Omega$, = 0.42 at $Z_f = 24\ \Omega$, and = 0.54 for ideal single cathode behavior, for the case with $V_{oc} = 15$ MV, $Z_a = 38\ \Omega$, $Z_o = 40\ \Omega$). The shift to lower diode impedance lowers the voltage at peak power. This model, simulation and data show that the power penalty for operating SABRE in positive polarity is greater than 25% compared to negative polarity (single cathode) operation, with a reduction in voltage at peak power of 28%.

Conclusions

This work has shown how well ion diodes can be coupled to positive polarity inductive adder MITLs. The best power efficiency requires an undermatched diode impedance, the level depending on the MITL operating impedance. Undermatching the diode impedance to the MITL self-limited impedance launches a reflected wave and allows recovery of cathode current. Understanding the scaling of positive polarity operation is needed to predict the ultimate efficiency of such systems. Agreement of several of the SABRE experimental observations and TWOQUICK simulations is a start in the direction of predictive capability.

Previous experimental data on HELIA, a short, four cavity positive polarity inductive adder with close-coupled electron [11] and ion diode [3] loads, showed that the MITL flow was indistinguishable from the single cathode model, given experimental uncertainties.

These experiments on SABRE with a transit-time-isolated applied-B ion diode load have shown that the maximum coupled power is best described by full gap flow with a Z_f of 20 Ω. The power penalty for operation of SABRE in positive polarity based on a simple model is 25% compared to negative polarity (single cathode) operation. The flow impedance increases along the extension MITL before the reflected wave returns to the monitor position. This effect is related to the loss of electrons to the anode, or return of electrons to the cathode. The HERMES-III experiments described in [17, 18] with a transit time isolated inverse pinch ion diode were also best described by the FGF limit at the adder exit.

We are improving signal timing accuracy, anode cable shielding and signal to noise, and developing time resolved voltage measurements to allow improved comparisons between simulation, model, and experiment.

Acknowledgment

The authors thank Mike Desjarlais for useful discussions.

References

[1] J. J. Ramirez, et al., Proceedings of the IEEE, 80, 946(1992).
[2] T. W. L. Sanford, et al., J. Appl. Phys., 67, 1700(1990).
[3] D. L. Hanson, et al., IEEE Trans. Plasma Science, 19, 831(1991).
[4] J. P. Corely, et al., 8th IEEE Pulsed Power Conference, 920(1991).
[5] D. L. Hanson, et al., 9th Inter. Conf. High-Power Particle Beams, (1992).
[6] C. W. Mendel, Jr., et al., Laser and Particle Beams, 1, 311(1983).
[7] P. A. Miller and C. W. Mendel Jr., J. Appl. Phys., 61, 529(1987).
[8] J. M. Creedon, J. Appl. Phys., 48,1070(1977).
[9] C. W. Mendel Jr., et al., J. Appl. Phys., 71, 3731(1992).
[10] S. E. Rosenthal, 1992 IEEE Conf. Plasma Sci.
[11] J. P. Corely, et al., 7th IEEE Pulsed Power Conference, 571(1989).
[12] M. S. Di Capua and D. Pellinen, J. Appl. Phys.,50, 3713(1979).
[13] A. V. Gordeev, V.V. Zazhivikhin, Sov.Phys.Tech.Phys., 25, 1363(1980).
[14] S. E. Rosenthal, C. W. Mendel, Bull. Amer. Phys. Soc., 34, 2143(1989).
[15] B. W. Church and R. N. Sudan, Bull. Amer. Phys. Soc., 36, 2362(1991).
[16] C. W. Mendel Jr., Bull. Amer. Phys. Soc., 37, 1535(1992).
[17] S. E. Rosenthal, IEEE Trans. Plasma Science, 19, 822(1991).
[18] D. L. Johnson, et al., 7th IEEE Pulsed Power Conference, 1989.
[19] B. W. Church, R. N. Sudan, 9th Conf. High-Power Particle Beams, (1992).
[20] J. E. Bailey, et al., Bull. Amer. Phys. Soc., 32,1873(1987).
[21] J. W. Poukey, and K. D. Bergeron, Appl. Phys. Lett., 32, 8(1978).
[22] T. D. Pointon, and D. B. Seidel, Sandia, private communication.
[23] S. E. Rosenthal, 1993 IEEE Conf. Plasma Sci.

DATE

FILMED

10/26/93

END